Growth structure of chemisorbed oxygen on GaAs(110) and InP(110) surfaces

K. A. Bertness,* J.-J. Yeh, D. J. Friedman, P. H. Mahowald, A. K. Wahi,
T. Kendelewicz, I. Lindau, and W. E. Spicer
Stanford Electronics Laboratories, Stanford University, Stanford, California 94305
(Received 24 December 1987; revised manuscript received 25 March 1988)

A study of oxygen chemisorption on GaAs(110) surfaces with both high-resolution synchrotron-photoemission spectroscopy and x-ray-photoemission spectroscopy of the oxygen 1*s* core level is presented in light of what can be learned about the atomic-scale structure during the growth of the first layers of oxide. Additional results for oxygen chemisorption on InP(110) are included for comparison with GaAs(110). Curve fitting of the synchrotron-photoemission data indicates that the spectra contain peaks due to direct oxygen bonding to semiconductor atoms, inducing large binding-energy shifts, as well as peaks arising from second-order charge transfer and structural relaxation, with smaller binding-energy shifts. These peak identifications are supported by the correlation between semiconductor and oxygen core-level intensities, the behavior of peak areas as a function of oxygen exposure, and the peak binding-energy spacings. The changes in intensity of the oxide peaks show that both Ga and As atoms are involved to an equal extent in the bonding with oxygen at coverages from 0.1 monolayers (ML) to at least 1.5 ML. Comparisons of the oxide peak areas for spectra taken with different surface sensitivity also demonstrate that oxygen chemisorption for InP and GaAs proceeds layer by layer, with large kinetic barriers to oxidation beyond the first two monolayers. The dominance of surface oxidation is confirmed by oxygen core-level spectroscopy and by calibration of the experimental surface sensitivity with surface-shifted peaks on the clean surface.

I. INTRODUCTION

The determination of the atomic-scale structure of chemisorbed oxygen on GaAs has been sought for many years, and this search has not been without controversy. Oxygen chemisorption on InP has induced less debate, but this relative quiet is due more to scarcity of data than simpler chemistry. The study of these two compound semiconductors is complicated by the fact that oxygen chemisorption destroys long-range order on the surface, as demonstrated for GaAs by the absence of new structure[1,2] in low-energy electron-diffraction (LEED) patterns. Much of the argument about specific bonding sites may therefore be due to the absence of strong preferential bonding, although detailed models such as those put forward by early workers[3,4] may be relevant to the short-range order on the surface. The current debate about oxygen chemisorption also extends to larger-scale structure concerning the degree to which oxygen chemisorption occurs only on the surface.

In this paper a variety of approaches will be taken in discerning the structure of the first one or two chemisorbed oxide layers of GaAs and InP, where the term "oxide" is used loosely since there is no strong evidence that bulklike oxides are formed for coverages of 1 or 2 monolayers (ML). After reviewing some of the work to date, including kinetics arguments with relevance to the structure, high-resolution core-level-spectroscopy data will be presented and discussed. The Ga 3*d* and As 3*d* core-level peaks are analyzed with a curve-fitting routine to determine the surface sensitivity for the experimental configuration used and to identify which parts of the spectrum can be associated with semiconductor atoms directly bound to oxygen. The data show that peaks with large binding-energy shifts relative to the bulk peak give the best correlation to oxygen uptake, while those with smaller binding-energy shifts are more likely due to structural relaxation in response to oxidation of nearby atoms. When designating those peaks with large chemical shifts as oxide peaks, the Ga and As oxide peaks areas show a one-to-one correspondence, suggesting that the oxygen chemisorbs in a mode which involves both Ga and As atoms. In contrast to some recent O 1*s* studies,[5,6] the shallow core levels (Ga 3*d*, As 3*d*, In 4*d*, P 2*p*) of InP and GaAs suggest that oxygen chemisorption on these compounds leads to similar growth structures, consisting of a few oxygen bonding sites with bond-angle or other minor structural variations. Finally, experimental evidence indicating that oxygen chemisorbs primarily on the surface of the semiconductor will be discussed. This evidence consists first of O 1*s* data which shows that there is too little O 1*s* signal to be explained by substantial subsurface oxidation, and, second, synchrotron photoemission work in which the electron escape depth is varied. The latter results agree only with structural models in which the oxygen binds to the first one to three layers of the semiconductor for both InP and GaAs. These models are used to calculate inelastic-scattering lengths for both semiconductors and the differences are discussed in terms of the scattering mechanisms predominant in the energy range of interest.

II. REVIEW OR PRIOR WORK

A. GaAs

Early work[1,4,7–13] in this field concentrated on observations of the saturation of oxygen uptake as a function

of exposure and absolute calibration of oxygen uptake from Auger and photoemission data. Several attempts have been made to identify the nature of the bonding, with evidence[4,8,10,12,13] for low-coverage (<0.1 ML) Ga-related sites and both As and Ga reactions during the main chemisorption phase. The reaction with molecular oxygen is now widely accepted[14–17] as being dissociative. The question of whether or not the oxygen chemisorption state consists of small patches of bulklike oxides (Ga_2O_3, As_2O_3) arose early in these investigations. Pianetta *et al.*[9] argued that chemisorbed oxides formed from molecular oxygen were not bulklike, since the use of excited oxygen led to oxides with different chemical shifts and also induced a loss of arsenic from the surface. The oxides formed with excited oxygen appear to be closer to the Ga-rich thick oxide films grown under conditions which are nearer to thermal equilibrium. Chemical depth profiling[18] of the interface between GaAs and bulk native oxide (30–40 Å thick) indicates that there are indeed differences between bulk oxides and the interfacial species. Bartels and Mönch[19] have seen changes in electron-energy-loss spectra at coverages between 0.6 and 1.0 ML which they attributed to the formation of two different oxide phases T_1 and T_2, with the structure of T_2 more similar to a bulklike oxide. Finally, Ludeke[8] proposed an amorphous surface oxide structure for coverages up to about 1 ML in which oxygen bonds to both Ga and As atoms, but segregation of the surface atoms into Ga_2O_3 or As_2O_3 patches does not occur. This view has been altered in later work with Landgren *et al.*[20] to a model of separate bulklike oxide phases which extend far into this semiconductor crystal.

B. InP

There have been fewer studies of the oxidation of InP with surface-analysis techniques on atomically clean substrates, most of which are synchrotron-radiation-photoemission studies[21–23] of the core-level shifts for the In 4*d* and P 2*p* core levels. As for GaAs, there is now clear evidence that both the group-III and group-V elements are participating in the oxidation reaction. There is some evidence[6] from O 1*s* core levels that oxygen chemisorption produces a single phase, most likely $InPO_4$, while other data[24] support formation of non-stoichiometric polyphosphates. The data discussed in this paper also argues for a lack of stoichiometry in the oxides formed, similar to the growth mode proposed for GaAs. Studies of thicker oxide layers grown anodically or thermally routinely observe indium oxides,[25,26] as is predicted by the In-P-O phase diagram.[27] The oxygen uptake for InP is generally slower than for GaAs,[21,28] and uptake on both semiconductors can be enhanced by the use of "excited" oxygen. For InP, however, the reaction rate is merely increased for excited oxygen exposures with no obvious changes in the photoemission spectra, in contrast to GaAs, where different chemical species are formed.

III. EXPERIMENT

The primary technique used in the experiments reported here is soft-x-ray-photoemission spectroscopy. Most of the spectra were collected at the new 4° line of the Stanford Synchrotron Radiation Laboratory using a grasshopper monochromator with a 600-lines/mm grating. Photon energies above 160 eV are generated using second-order light, which serves both to check the photon-energy calibration and improve the resolution of the spectra. A Physical Electronics cylindrical mirror analyzer (CMA) was used to measure the photoemitted electron-energy distribution with an analyzer pass energies of 10 or 15 eV and x-ray-photoemission (XPS) slits. This analyzer accepts electrons at a polar angle of 43° from its axis and over the entire 360° of azimuthal angle, and is thus partially angle-integrating. For synchrotron data the combined monochromator and CMA resolution is estimated from the Fermi-level edge of a thick gold film and used as the Gaussian width for clean surface spectra. Standard x-ray sources (Al anode, 148.6 eV; Mg anode, 1253.6 eV) were used to obtain O 1*s* spectra and the XPS Ga and As normalization spectra.

The samples are prepared by cleaving a rectangular bar with cross section 4×4 mm^2 in ultrahigh vacuum ($<2\times10^{-10}$ Torr), and an oxide layer equivalent to approximately 1 ML is then grown by exposing the surface to pure oxygen or nitrous oxide. Precautions taken against the direct excitation of the gases include keeping all ion gauges off from just before a fresh cleave until after all data for that cleave is taken, and evacuating the chamber to less than 10^{-7} Torr with a turbomolecular pump after exposure and before opening to the chamber ion pump. A typical experiment series consists of consecutive 10^4-, 10^6-, and 10^8-L [1 langmuir (L)$=10^{-6}$ Torr sec] gas exposures on the same cleave. Because of the wide variety of gas-exposure conditions and sample types used in obtaining the data discussed in this paper, the details of sample doping, temperature, oxidizing gas, and presence or absence of visible-light illumination are contained in Table I. Visible-light illumination is provided by an argon-ion laser operating in the continuous-wave, single-frequency mode with a photon energy of 2.41 eV (wavelength 514.5 nm); intensity figures are only accurate to about a factor of 2 due to the uncertainty in the overlap between the laser-beam Gaussian intensity profile and the area sampled by photoemission.

IV. KINETICS ARGUMENTS

Perhaps the strongest argument for surface oxidation without substantial subsurface oxide growth is the dramatic decrease in the oxygen sticking coefficient as coverage approaches approximately 1 ML. This phenomenon is illustrated by results from a number of workers in Fig. 1, where a linear exposure scale has been used to avoid the illusion of more gradual uptake when plotting against a logarithmic exposure scale. In all cases the uptakes saturates at about 1–2 ML, depending on how the researchers calibrate the oxygen uptake. To be precise, by saturation we mean that the sticking coefficient has dropped at least 5 orders of magnitude from its value at 0.5 ML, indicating a kinetic or thermodynamic barrier to further reaction. Such a barrier is easily explained if the oxidation takes place layer by lay-

TABLE I. Sample characteristic and preparation. Estimations of laser intensities have been revised (generally increased 2–3 times) from previously published work on the same samples. Where two temperatures are given, the value in parentheses is the temperature for the highest exposure (1×10^8 L), for which loss of the vacuum thermal insulation leads to an unavoidable temperature increase. [Here, 1 langmuir (L) $\equiv10^{-6}$ Torr sec.] Sample numbers are derived as follows: the first letter gives the doping type, the second letter gives the oxidizing gas (O for O_2, N for N_2O), the next three numbers give the sample temperature in kelvins, and the number after the hyphen gives the light intensity in W/cm^2.

Sample number	Doping density (cm^{-3}) and dopant	Oxidizing gas	Sample surface temp. (K)	Light intensity at 2.41 eV (W/cm^2)
1 (*n*O300-0)	$n=2.6\times10^{17}$, Si	O_2	300	0
2 (*n*O225-0)	$n=4.6\times10^{17}$, Si	O_2	225 (250)	0
3 (*n*O310-3)	$n=6.0\times10^{16}$, Si	O_2	310	3 to 2
4 (*p*O310-3)	$p=6.6\times10^{18}$, Zn	O_2	310	3 to 2
5 (*n*O320-9)	$n=6.0\times10^{16}$, Si	O_2	320	9 to 4
6 (*n*O225-15)	$n=4.6\times10^{17}$, Si	O_2	225 (260)	15 to 7
7 (*n*O185-10)	$n=2.6\times10^{17}$, Si	O_2	185	10 to 7
8 (*n*1N300-0)	$n=6.0\times10^{16}$, Si	N_2O	300	0
9 (*n*2N300-0)	$n=4.6\times10^{17}$, Si	N_2O	300	0
10 (*n*N200-0)	$n=4.6\times10^{17}$, Si	N_2O	200	0
11 (*n*N400-0)	$n=4.6\times10^{17}$, Si	N_2O	400	0
12 (*n*N320-7)	$n=2.6\times10^{17}$, Si	N_2O	305	7 to 4

er, since oxidation of the first and possibly second layers of the GaAs crystal requires breaking relatively few bonds with the possibility of further energy reduction by surface structural relaxation. Oxidation of deeper layers is also expected to be limited by diffusion of the reactant gas and/or semiconductor atoms.

The leading alternative to this model is one in which microfissures or defects in the crystal face act as extensions of the surface layer, and thus allow oxidation to take place well below the average surface position. This type of model, although used[20] to explain evidence for subsurface oxidation from curve fitting of Ga 3*d* peaks at low oxygen coverage, does not easily explain the kinetics observed. Uniformity in depth and density of the defects or fissures would be needed to account for the saturation effect seen in Fig. 1. Aside from the arguments questioning the need to postulate microfissures, direct evidence against their existence can be found in recent scanning-tunneling-microscopy work.[29,30] These studies find no evidence for fissures on cleaved surfaces and demonstrate that oxygen does react with "perfect" GaAs(110) surfaces.

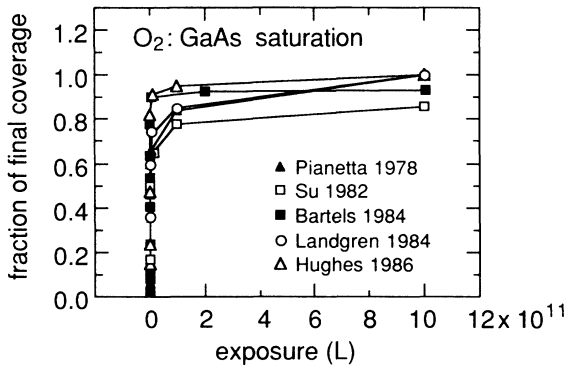

FIG. 1. Saturation of oxygen uptake vs gap exposure (linear scale). Although a logarithmic scale will show that oxygen uptake is not completely halted, this graph using a linear scale demonstrates the dramatic decrease in sticking coefficient near a coverage of 1 ML (ML denotes monolayer). Final coverages (at 10^{11} L) reported by each group are 0.5, 1.0, 0.82, 0.67, and 1.7 ML for Pianetta *et al.* (Ref. 9), Su *et al.* (Ref. 4), Bartels and Mönch (Ref. 19), Landgren *et al.* (Ref. 20), and Hughes *et al.* (Ref. 5), respectively. [Here, 1 langmuir (L) $\equiv10^{-6}$ Torr sec.]

V. HIGH-RESOLUTION CORE-LEVEL SPECTROSCOPY

The early work in this field favored a metastable surface oxide made by random insertion of oxygen atoms into existing Ga—As bonds (primarily surface bonds), as opposed to separate domains of the bulklike oxides Ga_2O_3 or As_2O_3. More recent photoemission work has challenged this interpretation through the detection of additional peaks in the spectra of both the clean and oxidized surfaces of III-V, compound semiconductors, made possible by improved resolution in synchrotron-light sources and electron-energy analyzers. Landgren *et al.*[20] use their results to justify a model of oxygen chemisorption in which bulklike oxides form with substantial subsurface oxidation even at submonolayer coverages. The presence of separate Ga and As oxide phases is deduced from differing growth rates in the intensities for those peaks attributed to gallium oxides and those attributed to arsenic oxides. In this section, both the subsurface-oxide and separate-phase growth-mode hypotheses are disproved, and a new peak classification scheme is presented which attributes peaks with small binding-energy shifts to structural relaxation (akin to the effects which produce surface shifts) and designates only peaks with large chemical shifts as representative of direct oxygen bonding. While Landgren's work demonstrates that

the oxygen-induced peaks in the Ga and As core-level spectra are too broad to be attributed to a single atomic bonding site, the Landgren peak-classification scheme ignores the role of structural relaxation, which is significant in an amorphous oxide such as this one.

A. Surface sensitivity and surface shifts for GaAs

In 1980 Eastman *et al.*[31] reported photoemission spectra for GaAs with sufficient resolution to distinguish surface peaks with different binding energies relative to emission from the underlying bulk atoms. Since for a well-ordered surface almost all of the atoms at the surface will have undergone the same reconstruction, the fractional area r_{surf} of the surface peaks, defined as the ratio of surface peak area to the total peak area, gives a measure of the contribution of surface atoms to the overall photoemission spectra. The value of r_{surf} will be different for photoemission spectra covering different kinetic-energy ranges due to the change in electron inelastic-scattering lengths. To extract the peak areas, we have applied a curve-fitting routine which uses a nonlinear regressive least-squares algorithm to optimally fit the spectral with a theoretical line shape consisting of a spin-orbit doublet, each component of which is a convolution of a Gaussion peak and a Lorentzian peak. The Gaussian widths are fixed for each fit and, for the clean surface, are taken from the combined resolution of the photon source and electron-energy analyzer. When the same routine is used for heavily oxidized surfaces, we find that the nonuniformity of chemical and structural environments require the use of larger Gaussian linewidths in order to maintain good reduced χ^2 values and consistent results from exposure to exposure. The parameters used in the curve fitting are given in Table II.

When analyzed for surface peaks, data for clean and almost clean spectra of GaAs yield spectral deconvolutions such as those illustrated in Fig. 2. The binding-energy differences $\Delta E = E_{bulk} - E_{surface}$, observed are 0.28 eV for the Ga 3*d* core level and -0.37 eV for the As 3*d* core level, which are within 0.01 eV of earlier results.[31,32] The fractional area in the surface peak, r_{surf}, however, tends to vary from surface to surface for spectra taken near maximum surface sensitivity in the (35–38)-eV kinetic-energy range. When comparing r_{surf} for the Ga and As core levels on the same cleave, however, it becomes apparent that the mean value of r_{surf} for Ga and As is relatively constant, as illustrated in Fig. 3. This observation suggests that nonuniform Fermi-level pinning has caused a portion of the spectrum to be shifted slightly in the same direction for both core levels, therefore causing an increase in one surface peak while causing a decrease in the other. This hypothesis is further supported by the fact that for one *p*-type GaAs sample, the Ga r_{surf} appears to be larger than the As r_{surf}, while the opposite is true for *n*-type GaAs since Fermi-level pinning causes shifts in opposite directions for the two doping types. Finally, the spectra for 10^4-L O_2 exposures show considerably less variation. This exposure is low enough that no oxide peaks can be detected, but that Fermi-level pinning is complete for *n*-type samples. Small doses of oxygen have previously been observed to increase uniformly in work function[33] and to sharpen[34] valence-band features.

Based on the data in Fig. 3, the surface sensitivity for the experiments described in this work is such that $r_{surf} \approx 0.48 \pm 0.04$ for electrons with kinetic energy of about 38 eV relative to the valence-band maximum; in other words, 48% of the emission in the spectra comes from the surface layer. This value gives more weight to those points in Fig. 3 for which the Ga and As r_{surf} values are approximately equal. From this value we calculate an electron inelastic-scattering length of 4.2 ± 0.5 Å based on the standard model in which the surface atoms contributing to the surface peaks constitute exactly 1 ML. The difference from work reported by other groups[20,31,32] is explained[35] simply by the difference in angular acceptance of the electron-energy analyzers used.

B. Identification of oxide peaks for GaAs

Typical results from the curve fitting of photoemission spectra for oxidized surfaces are illustrated in Fig. 4. The spectra show that both the Ga 3*d* and As 3*d* core levels undergo distinct changes due to oxygen chemisorption, although the chemical shifts for the As 3*d* core level are larger and therefore more easily resolved than the Ga 3*d* shifts. The spectra in Fig. 4 are taken from surfaces which have been exposed to oxygen in the presence of visible light; the use of laser light,[36–38] however, does not alter the shapes of the oxidized core-level spectra from the shapes seen[4,9] after room-temperature oxygen chemisorption in the dark. Moderate cooling during laser-assisted oxygen exposure of the sample also does not affect the spectral line shape, as can be seen by comparing Fig. 4 and other spectra taken under similar conditions[35] with spectra taken after room-temperature exposures such as those mentioned above and those illustrated in Figs. 7(a) and 7(b). The use of nitrous oxide[37] as the oxidizing agent, on the other hand, will change the shape of the As 3*d* spectra, and this condition is thus the only experimental variable in this study (see Table I) which results in noticeably different chemical species.

For purposes of identification, the shifted peaks are divided into two groups—the small-shift peaks which are chemically shifted less than 0.5 eV for the Ga 3*d* core level and less than 0.7 eV for the As 3*d* core level, and the large-shift peaks with larger chemical shifts. The large-shift peaks can be unambiguously identified with oxygen bonding, since these peaks grow monotonically with increasing oxygen exposure and have binding energies similar to those found[39,40] in the bulk oxides Ga_2O_3 and As_2O_3. The identification of the small-shift peaks is more difficult, but here it will be shown that these peaks are most logically attributed to structural relaxation and second-order charge transfer involving semiconductor atoms near but not directly bonded to oxygen. The strongest evidence comes from the O 1*s* data presented in Sec. VI, where it is seen that the large-shift peak areas have a linear correspondence to the O 1*s* peak areas, while the inclusion of small shift peaks weakens the correlation. In this section other features related to the

peak areas and binding energies will be seen to support these peak identifications as well.

The behavior of the peak areas as a function of oxygen exposure, for example, suggests that the small-shift peaks are due to direct oxygen bonding. In Fig. 5 the fractional peak areas for a typical spectral series are plotted against oxygen exposure for individual peaks with various binding energies relative to the bulk peak as described in Table II. The large-shift peaks clearly increase as a function of oxygen exposure, reaching a fractional peak area slightly greater than the fractional peak area corresponding to the mean surface peak area for the clean surface, indicating that the final coverage is roughly 1 ML, and possibly more. (The absence of emission from the 2.6-eV oxide peak at 10^6 L may not be significant as there is too little oxide emission to allow easy resolution from the other oxide peak.) As one would expect, the surface peak area for the As 3*d* core level has gone to zero by the time the coverage reaches 1 ML; a different small-shift peak appears instead with binding energy 0.26 eV greater than the bulk peak. The latter peak has its greatest area at intermediate coverage, and decreases to about 0.2 fractional peak area for 1-ML coverage. These nonmonotonic changes in peak area suggest a nearest-neighbor effect wherein As atoms bound to oxidized Ga atoms experience a small binding-energy shift. When the surface is

TABLE II. Curve-fitting parameters used for oxygen chemisorption on GaAs. Parameters for which a range is given are optimized by the curve-fitting routine. The line shape used is a spin-orbit doublet, each component of which is a convolution of a Gaussian peak and a Lorentzian peak with the widths given. All spectra analyzed with curve fitting were taken at the photon energies represented here.

Ga 3*d*

Substrate binding energy (relative to valence-band maximum), $j=\frac{5}{2}$: 18.7±0.1 eV
Spin-orbit energy splitting, $(j=\frac{5}{2})-(j=\frac{3}{2})$: 0.44 eV
Spin-orbit amplitude ratio, $(j=\frac{5}{2})/(j=\frac{3}{2})$: 1.5
Background: exponential with decay constant 0.27 eV

Spectral decompositions ($h\nu=60$ eV)	Binding energy relative to bulk peak (eV)	Gaussian FWHM (eV)	Lorentzian FWHM (eV)
Clean and low exposure			
Peak 1, bulk	≡0	0.34[a]	0.2±0.05
Peak 2, surface	0.28±0.02	0.34[a]	0.25±0.05
Oxidized			
Peak 1, bulk	≡0	0.34[a]	0.2 to 0.35
Peak 2, surface, relaxation?	0.27 eV (0.32±0.1)	0.34[a]	0.1 to 0.4
Peak 3, oxide	0.9 eV (0.8±0.2)	0.8	0.4 to 0.7

Reduced χ^2 1.5 to 3.0, up to 4 for clean spectra

As 3*d*

Substrate binding energy (relative valence-band maximum), $j=\frac{5}{2}$: 40.5±0.1 eV
Spin-orbit energy splitting, $(j=\frac{5}{2})-(j=\frac{3}{2})$: 0.70 eV
Spin-orbit amplitude ratio, $(j=\frac{5}{2})/(j=\frac{3}{2})$: 1.5
Background: manual correction for plasmon background, linear during fits

Spectral decompositions ($h\nu=80$ eV)	Binding energy relative to bulk peak (eV)	Gaussian FWHM (eV)	Lortzian FWHM (eV)
Clean and low exposure			
Peak 1, bulk	≡0	0.41[b]	0.12 to 0.26
Peak 2, surface	−0.37±0.03	0.41[b]	0.2 to 0.5
Oxidized			
Peak 1, bulk	≡0	0.41[b]	0.3 to 0.5
Peak 2, relaxation? (N_2O)	−0.6±0.1	0.6	0.2 to 0.4
Peak 3, relaxation? (O_2)	0.26±0.1	0.6	0.1 to 0.4
Peak 4, oxide (N_2O)	1.1±0.3	0.6	0.35 to 0.6
Peak 5, oxide	2.6±0.2	0.6	0.3 to 0.5
Peak 6, oxide (O_2)	3.1±0.15	0.8	0.1 to 0.3

Reduced χ^2 1 to 3, up to 5 for clean spectra.

[a]Gaussian width 0.42 eV for runs using 15-eV analyzer pass energy instead of 10 eV.
[b]Gaussian width 0.50 eV for runs using 15-eV analyzer pass energy instead of 10 eV.

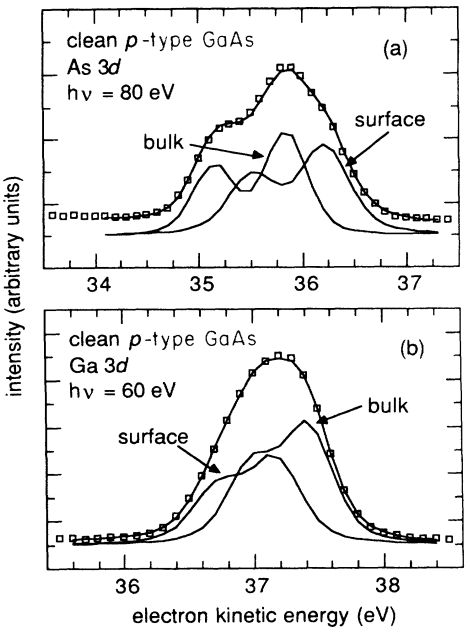

FIG. 2. Photoemission spectra illustrating surface peaks on GaAs(110). The binding-energy shifts for the surface peaks relative to the bulk peaks are -0.37 and 0.28 eV for (a) the As $3d$ core level and (b) the Ga $3d$ core level, respectively. Kinetic energies relative to the valence-band maximum (VBM) are approximately 5 eV higher. Note that the surface contributes almost half of the entire emission to each spectrum. Data are from sample 4 (pO310-3), and are taken with an analyzer pass energy of 10 eV.

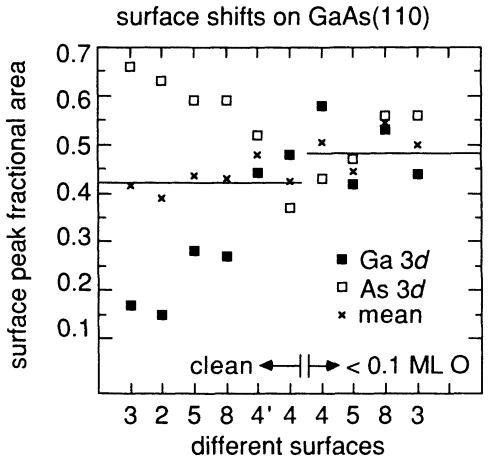

FIG. 3. Normalized surface peak areas on GaAs(110) for various samples. Values are taken from curve fitting of spectra with $\approx$37 eV electron kinetic energy, which is equivalent to $\approx$42 eV kinetic energy above the VBM. Although the mean value of the surface peak area is relatively constant, nonuniformity in Fermi-level pinning at the surface creates peak area deviations of opposite sign for As $3d$ and Ga $3d$ core levels. Low exposures of oxygen improve Fermi-level uniformity and thus improve the agreement between the surface peak areas for the two core levels. Sample 4′ is from the same piece of GaAs as sample 4 but was not used in an exposure series.

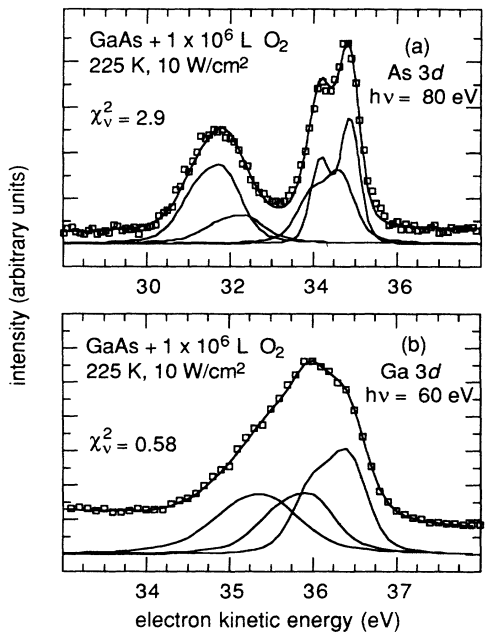

FIG. 4. Examples of curve fitting for As $3d$ ($h\nu=80$ eV) and Ga $3d$ ($h\nu=60$ eV) core levels after oxygen chemisorption on GaAs, sample number 2 (nO225-15). The oxygen exposures for this sample were accomplished with a sample temperature of 225 K and under illumination with visible light of about 15 W/cm^2. Since these spectra have the same line shapes as those taken from samples exposured to oxygen at room temperature both with and without visible light, one may conclude that these variables do not affect the final bonding structure of the oxide. Spectra are taken with an analyzer pass energy of 15 eV.

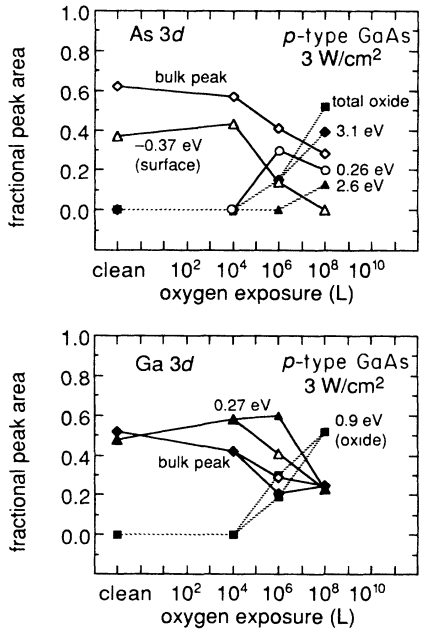

FIG. 5. As $3d$ and Ga $3d$ core-level fractional peak areas as a function of exposure to molecular oxygen for sample 4 (pO310-3). The binding-energy shifts relative to the bulk-peak are indicated for each peak used in curve fitting. Peaks attributed to direct oxygen bonding are connected with dashed lines. The open symbols for Ga $3d$ data (lower panel) give the results of curve fitting in which the oxide peak binding-energy shift is not constrained to be at least 0.85 eV.

partially oxidized, both unoxidized surface atoms and second-layer atoms will contribute to the peak, but once the surface becomes completely oxidized only the second layer will contribute. The final fractional peak area of this peak is close to the expected 24% contribution to the spectrum from the second layer.

For the Ga 3*d* core level, the picture is not quite so clear because of the small binding-energy shifts involved. Again, the large-shift peak at about +0.9 eV greater binding energy than the bulk peak can be identified as Ga bound directly to oxygen, since the area of this peak increases monotonically with oxygen exposure. At intermediate oxide coverages, the curve-fitting program often arrives at an oxide peak whose binding energy is about 0.2 eV less than the oxide peak binding energy at 1 ML, so the results of constrained fits which maintain the larger binding-energy shift (0.9 eV) are probably closer to the true concentrations of oxidized surface atoms. (An example of constrained and unconstrained fits is given in Fig. 3.4 of Ref. 38; there is no significant difference in the χ^2 values for the two types of fits.) The small-shift peak at about +0.3 eV arises from the surface atoms for the clean surface and first exposure, but does not disappear even when the coverage has reached 1 ML. This persistence indicates that another Ga site is being formed with nearly the same binding energy as a clean surface site. The increased emission at intermediate coverage echoes the behavior of the 0.26-eV peak in the As 3*d* spectrum and, by the same arguments given above, indicates that the new site may be a Ga atom bonded to an oxidized As. By the final exposure the surface contribution is no longer present and only these nearest-neighbor atoms contribute, again with a fractional peak area corresponding to the expected contribution of second-layer atoms. While the intensity behavior of the 0.27-eV peak would also be expected from a Ga site consisting of a Ga atom bonded to only one oxygen atom, O 1*s* data indicate that there is no correlation between oxygen coverage and the 0.27-eV peak area.

A second reason to regard the small-shift peaks as structural relaxation shifts comes from the inability of the "ligand-shift" model to explain the observed sequence of binding-energy shifts. In this model the net binding-energy shift for a semiconductor atom is assumed to be the product of the binding-energy shift for an —O ligand replacing a bond to another semiconductor atom times the number of such oxygen replacements which occur. It can be seen in Table II, however, that for both Ga and As the smallest shifts are well below half the next-larger shifts. The corresponding peaks are therefore unlikely to be due to suboxide formation, that is, sites with a single oxygen atom attached to a semiconductor atom which otherwise is bound only to semiconductor atoms. The absence of suboxides in itself is interesting since it implies that oxygen chemisorption is immobile with both oxygen atoms from the oxygen molecule bonding at the dissociation site.

The absence of a suboxide peak for molecular oxygen exposures is further demonstrated by the appearance of such a peak at 1.1 eV greater binding energy relative to the bulk peak in As 3*d* spectra for surfaces oxidized with nitrous oxide.[37] Since N_2O releases only one oxygen atom per reacting molecule, the growth of a suboxide where none exist for O_2 chemisorption is not surprising. This change in structure also affects the As 3*d* small-shift peaks by inducing a weak peak at about −0.6 eV lower binding energy (not shown here; see Fig. 3.4 of Ref. 38). The 0.26-eV peak seen after O_2 exposures cannot be resolved in the N_2O spectra, so the corresponding site has either disappeared or is obscured by the 1.1-eV peak. The −0.6-eV peak also has its greatest intensity at intermediate coverage, but never exceeds 0.1 fractional peak area. The Ga 3*d* spectra are indistinguishable for N_2O and O_2, so the difference in growth structure seems to be related chiefly to structural relaxations and the bonding between oxygen and arsenic.

A final reason for attributing small-shift peaks to structural relaxations and second-order charge transfer is that the energy shifts are of exactly the magnitude expected for these processes. The surface shifts described in the preceding section with magnitudes of a few tenths of an eV are the result of interplay between bonding charge transfer (affecting the potential due to the shielded nucleus at a lattice site) and structural relaxation (affecting the Madelung potential[41] due to surrounding nuclei). Since unoxidized atoms in the first and second layers of a partially oxidized surface undergo similar changes at least as great as those in surface reconstructions, unoxidized atoms should also experience similar binding-energy changes. Theoretical calculations[42] predict a Ga 3*d* binding-energy shift of 0.8 eV for a Ga atom attached merely to an oxidized As atom, not to an oxygen atom itself, based on the redistribution of charge following the addition of highly electronegative oxygen atoms[43] to a model semiconductor molecule. The increased width of the photoemission peaks, especially peaks attributed to oxides, is also explained by deviations from a perfectly ordered chemisorption oxygen structure, thereby creating a distribution of binding-energy shifts.

Using these peak assignments, one can then compare the oxide peak areas for the Ga 3*d* core level with the corresponding peak areas in the As 3*d* spectra. In Fig. 6 these areas are shown to have an approximate 1:1 correspondence over the entire exposure range studied. The scatter in the data is improved by constraining the Ga peaks to the binding energy shifts of 0.27 and 0.9 eV. A linear least-squares fit of the constrained Ga results does indicate that there is somewhat less Ga oxide than As oxide, but the difference is smaller than the estimated uncertainty of 20% for Ga 3*d* peak-area determinations. (The uncertainty for As 3*d* spectra peak areas is 4%.) This correspondence supports growth-structure models in which equal amounts of Ga and As atoms participate in the reaction with oxygen. Surface-growth models such as the O=As—O—Ga structure put forth by Su *et al.*[4] are consistent with this picture, but a model of Ga_2O_3 island nucleation with unoxided As patches is not.

C. Comparison of InP and GaAs

Hughes *et al.*[5,6] have proposed that while oxygen chemisorption on GaAs produces a highly disordered

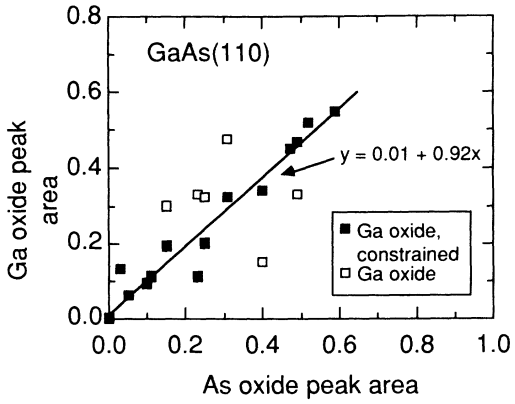

FIG. 6. Correlation of oxide (large-shift) peak areas for Ga $3d$ and As $3d$ core levels. The areas of peaks with the large binding-energy shifts (>1.0 eV for As $3d$ and >0.5 eV for Ga $3d$) have a one-to-one correspondence, indicating that oxygen uptake involves both semiconductor constituents to a more or less equal extent. Constrained fits (solid squares) are those for which the Ga oxide peak is at least 0.85 eV from the bulk peak. At low and high coverage the Ga peak binding energies meet this condition without constraining the curve fitting routine. Data from samples 3 (nO310-3), 4 (pO310-3), 5 (nO320-9), and 8 (n1N300-0) are included; see Table I for details.

mixed-phase structure, oxygen chemisorption on InP forms a simpler, single-phase product consisting mostly of $InPO_4$. This conclusion is based to a large extent on O $1s$ core-level spectroscopy, which indicates two components for the O $1s$ core level for oxygen chemisorbed on GaAs but only one component for oxygen chemisorbed on InP. The semiconductor core-level spectra for GaAs and InP, however, are virtually identical in the number of oxide peaks and degree of core-level broadening following oxidation, as illustrated in Fig. 7. This similarity argues strongly against a single-phase –versus–double-phase hypothesis since the InP core-level components should be fewer and less broad if the InP chemisorbed oxide had a simpler, more ordered structure than oxidized GaAs. An alternative explanation consistent with both core-level and O $1s$ results is that both semiconductors oxidize in a way which produces structural disorder but falls short of breaking up the semiconductor lattice into separate oxide phases. The two O $1s$ peaks observed for GaAs may correspond to two different oxygen bonding environments such as As=O and As—O—Ga. For InP the equivalent oxygen bonding sites may be coincidentally closer to one another in binding energy and occur in different relative quantities. The bond-energy difference between an anion-

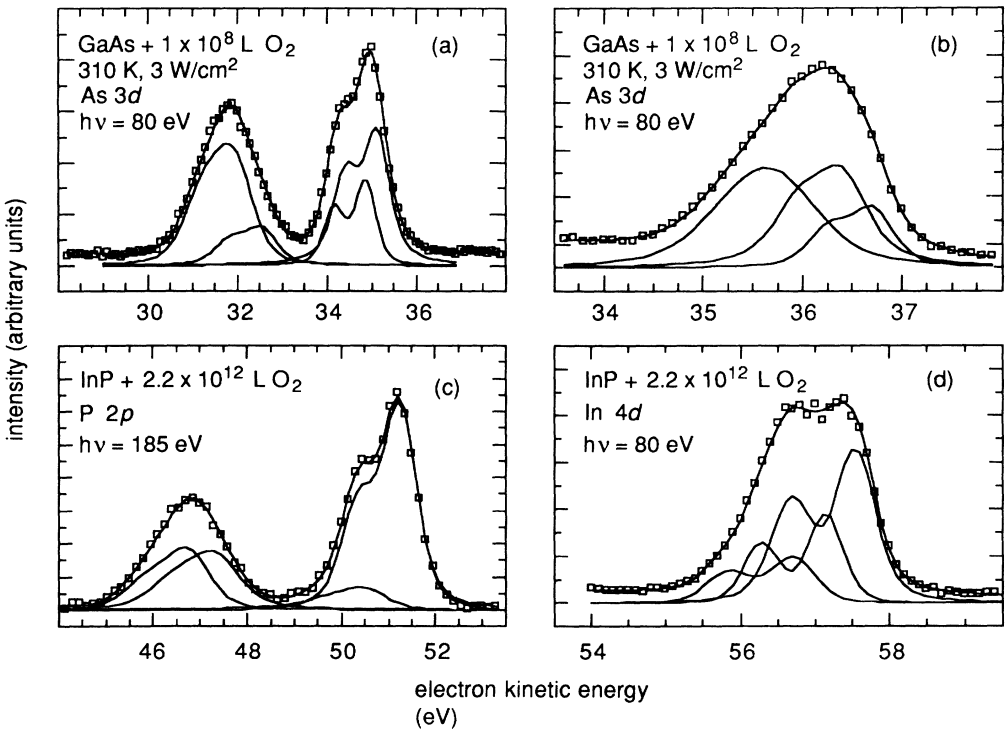

FIG. 7. Comparison of core-level spectra for oxidized GaAs and InP. The similarity in peak widths and number is consistent with similarity in structural inhomogeneity for the two semiconductors. Data in (a) and (b) are from sample 3 (nO310-3) taken with resolutions of 0.44 and 0.34 eV, respectively. Samples used for (c) and (d) are Sn-doped InP with $n=5\times10^{17}$ cm^{-3} under experimental conditions such that the spectral resolution is 0.65 and 0.35 eV, respectively. As for the GaAs curve fits, oxidation of the InP surface leads to peaks broadened beyond the experimental resolution; full details of the InP curve fitting can be found in Ref. 38.

oxygen-cation bond and an anion-oxygen double bond is, in fact, estimated[44] to be 1.7 times less for InP than for GaAs at 1.84 and 3.06 eV, respectively. Our picture of a nonstoichiometric blend of oxides therefore agrees with the work of Hollinger *et al.*[24] on thermally and anodically grown oxides.

The difference in oxygen-semiconductor phase diagrams is also often used to justify different growth structures for oxygen chemisorption on InP and GaAs. In particular, the absence of a tie line between $GaAsO_4$ and GaAs in the Ga-As-O equilibrium phase diagram[45] suggests a driving force toward separate oxide phases, whereas the equivalent compounds for InP can coexist[27] at equilibrium. This argument fails because the species formed during room-temperature oxygen chemisorption on GaAs are not in thermodynamic equilibrium with each other or with the oxygen gas overpressure present during the exposures. Thurmond *et al.*[45] note, for example, that even at 500 °C the attainment of equilibrium phases is incomplete after 48 h; the reaction rates leading to the decomposition of $GaAsO_4$ are therefore negligibly small under the conditions of the experiments described here. Furthermore, the room-temperature oxygen chemisorbed state is known to be unstable with respect to moderate heating[4,5] (about 350 °C) and exposure to excited oxygen.[9] The phase-diagram work on InP is also based on data obtained at higher temperatures (600 °C and above) where kinetic factors have negligible influence, although the absence[22] of an excited oxygen effect does suggest that room-temperature chemisorbed oxides on InP may be close to equilibrium.

VI. O 1*s* DATA

The oxygen XPS data for the same GaAs surfaces studied with high-resolution core-level spectroscopy also support the identification of large-shift peaks with oxides and small-shift peaks with structural relaxation. In Fig. 8 the fractional peak areas for the large-shift As 3*d* peaks ($\Delta E > 1.0$ eV) are shown to be in approximate 1:1 correspondence with the oxygen coverage measured from the O 1*s* areas. Differences between N_2O and O_2 are probably due to systematic error in photoionization cross sections since the N_2O data are taken with an Al $K\alpha$ x-ray source, while O_2 data are taken with a Mg $K\alpha$ source. The largest deviations from this correlation are at low coverages, where the O 1*s* data indicate more oxygen on the surface than appears in the As 3*d* spectra, particularly for those exposure series made with molecular oxygen in the dark. This extra oxygen could be oxygen bound to defect Ga sites as previously observed,[4,19] or may be a weakly bound chemisorption state.[19,28]

Some of the data are examined in more detail in Fig. 9, which illustrates the scatter induced by including the peaks with small binding-energy shifts. A linear least-squares fit for each data set shows that the large-shift peaks have a greater linear correlation factor R with the O 1*s* data than linear fits which include small-shift peaks. Since the surface peak for the Ga 3*d* core level overlaps with the low-binding-energy-shift peak for Ga 3*d*, the unusually high small-shift peak areas are to be expected at low coverages. To overcome this complication, data points are also shown for which the surface contribution

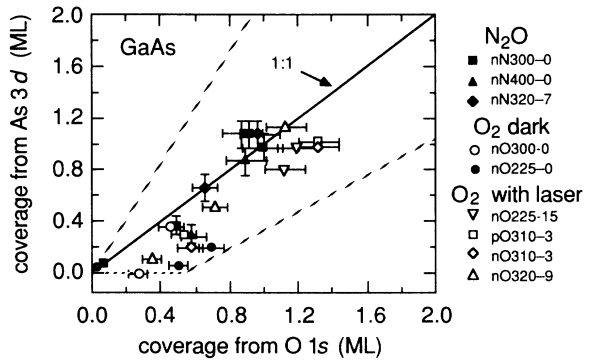

FIG. 8. Correlation of As oxide (large-shift) peak areas with O 1*s* peak areas. The rightmost limits dashed line corresponds to an oxide thickness of 2 Å and the leftmost to 4 Å. The data show a linear dependence between the large-shift (1.0 eV or more) As and O 1*s* peak areas for the higher coverages with some evidence for oxygen not detected in the As peaks at low coverage, particularly for molecular oxygen exposures in the dark (circles). Sample numbers refer to samples 9, 11, 12, 1, 2, 6, 4, 3, and 5, from top to bottom, in Table I.

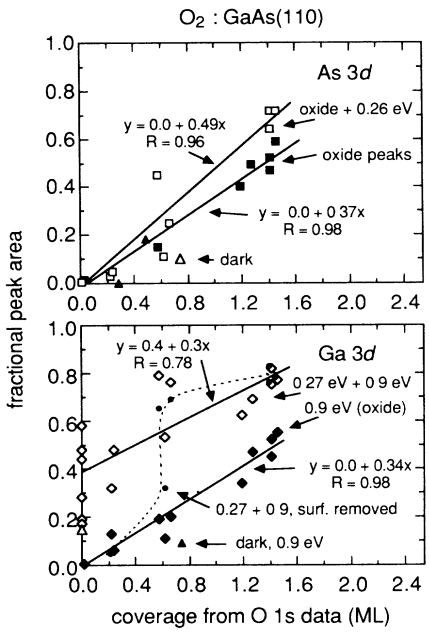

FIG. 9. Correlation between O 1*s* peak areas and large-shifted Ga 3*d* and As 3*d* peaks. The inclusion of small-shift peaks (open squares and diamonds) weakens the good correlation between O 1*s* peak areas and semiconductor "oxide" peak areas (solid squares and diamonds), indicated by a decrease in the linear correlation parameter R from a least-squares fit. The disagreement between O 1*s* peak areas and the sum of both shifted peak areas for Ga 3*d* is not improved by removing the estimated surface-peak contributions (solid circles). Error margins and oxygen coverage determination are the same as those in Fig. 8; the O 1*s* coverage scale assumes a 2-Å-thick oxide layer. Data from samples 3 (*n*O310-3), 4 (*p*O310-3), 5 (*n*O320-9), and 8 (*n* 1N300-0) are included.

has been removed by subtracting the As 3*d* surface fractional peak area from the sum of the Ga 3*d* 0.27 and 0.9-eV fractional peak areas; as illustrated, however, this procedure does not remove the scatter introduced by adding the small-shift peak. The disagreement between the O 1*s* data and the sum of the small-shift and large-shift peaks cannot be explained by independent growth modes for Ga and As since the deviations from linearity are in the same directions for both the Ga 3*d* and As 3*d* peaks.

Another conclusion which is supported by the O 1*s* data is that oxygen chemisorbs only to the first atomic layer or so of the GaAs(110) surface. The oxygen coverage may be calculated from the O 1*s* peak areas normalized to Ga and As 2*p* and 3*d* peak areas for which the spectra are taken with either a Mg- or Al-anode x-ray source. Several corrections are involved in making this comparison, as detailed in the Appendix, but the most problematic is the thickness over which the oxygen is assumed to be distributed. The dashed lines in Fig. 8 demonstrate where the values for the O 1*s* coverage would tend to line up as this thickness is changed from 4 Å (leftmost line) to 2 Å (rightmost line). Although greater thicknesses can be modeled, one can see that even for a 4-Å layer thickness the O 1*s*–derived coverage is only two-thirds of the synchrotron As 3*d*–derived coverage. The O 1*s* spectra are taken under conditions where the inelastic scattering length is about 18 Å, so any oxygen a few layers below the surface is being detected. Since there is no way to reconcile a counting of more As atoms with large binding-energy shifts than oxygen atoms, the oxygen must be no more than 4 Å into the surface for growth. In fact, *two* oxygen atoms per arsenic atom are probably needed to produce shifts greater than 1.0 eV, in which case most of the oxygen atoms must be within 2 Å of the surface. The assumption of a columnar growth mode (see next section) does not extend the possible oxygen bonding depth any farther, since the fraction of each layer which is oxidized cannot be lower[46] than the observed As oxide fractional peak area, here 0.5 at the highest exposure. A typical oxygen coverage in each lattice plane therefore cannot be below 0.5 ML, a condition which is violated when the oxide layer is assumed to be 6 Å or more thick.

VII. VARIATION OF ELECTRON INELASTIC-SCATTERING LENGTHS

Additional information about the oxide growth structure can be obtained by taking advantage of the fact that the inelastic-scattering length for electrons in a solid is a function of their kinetic energy. With a tuneable light source such as synchrotron radiation, the photon energy can be changed to vary the kinetic energy of electrons from a particular core level and thus change the photoemission probing depth. If the oxidized atoms are near the surface, then the relative contribution of the oxide peak(s) to the entire spectrum will be small at low kinetic energy, where the scattering length is long and many of the underlying unoxidized atoms contribute. The maximum oxide contribution will be found when the scattering length reaches its minimum, and finally the relative shifted area will decrease again at high kinetic energy, where the scattering length begins to increase. This trend can be seen in Fig. 10 in comparing the relative size of the oxide peaks in panels (a)–(c), confirming the fact that the scattering length is changing relative to the oxide thickness over the kinetic-energy range covered. Note that the minimum inelastic-scattering length of about 4.3 Å occurs for the kinetic-energy range represented in Fig. 10(b).

The degree of surface and subsurface oxidation can be determined quantitatively by examining the oxide fractional peak area, r, defined as the ratio of the area of the oxide peak to the total area under the curve. In Fig. 11(a) the oxide fractional peak areas r are presented for the same surface at several photon energies for two experiments (one of which has been reported[35] previously) on GaAs and one on InP. Because the oxide contribution is well resolved from the bulk contribution, this ratio has been determined simply by numerically calculating the area under the respective peaks as illustrated in Fig. 10(c). Before computing areas it is necessary to manually apply a combination of linear and iterative background subtractions which attempt to approximate the clean spectra background. The As 3*d* core level is unfortunately near a broad plasmon feature[47] which is not easily modeled by simple functions. For purposes of comparison with the results of other experiments, the kinetic-energy scale is defined relative to E_v, the valence-band-maximum energy. The kinetic energy relative to the analyzer work function is smaller than the kinetic energy relative to E_v by the sum of the analyzer work function and the energy of the Fermi level relative to E_v, with a typical difference being 5.5 eV.

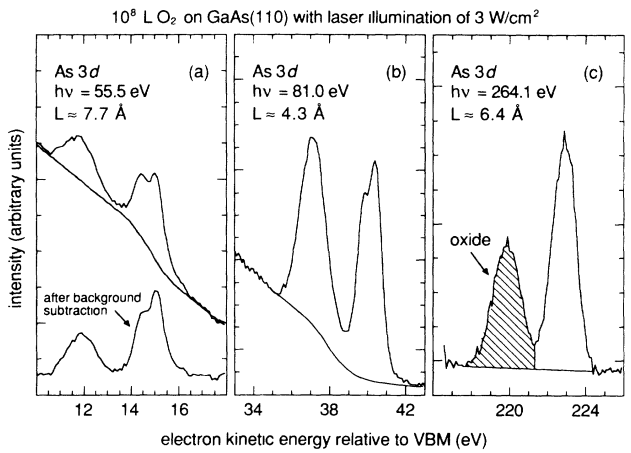

FIG. 10. Photoemission spectra of oxidized GaAs for the As 3*d* core level at three representative photon energies showing how the contribution of the oxide peak intensity changes relative to the unoxidized peak as the scattering length L first decreases and then increases again. The surface [sample 4 (pO310-3)] was exposed to 1×10^8 L O_2 with simultaneous laser illumination of about 3 W/cm^2, yielding a coverage equivalent to a 10^{13}-L O_2 exposure in the dark. (a) and (b) illustrate typical background subtraction techniques, and (c) shows an example of how the spectra are divided into oxidized (shaded area) and unoxidized peaks.

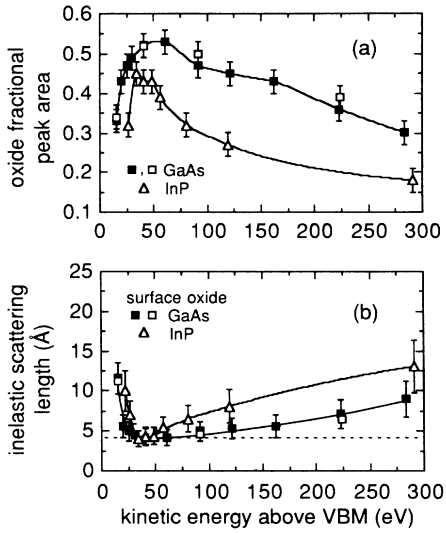

FIG. 11. (a) Oxide fractional peak areas and (b) inelastic-scattering lengths for GaAs and InP. Electron inelastic-scattering lengths are calculated self-consistently with a surface-structure model as described in Sec. VII. The differences between InP and GaAs can be explained in terms of the energy dependence of photoionization cross sections. The dashed line in (b) indicates the scattering length measured from the GaAs clean surface at ≈42 eV above the VBM.

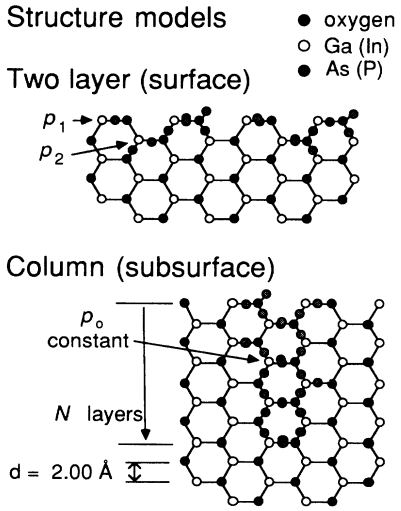

FIG. 12. Oxide-growth models, two layer and columnar. The two-layer models assume that oxygen is present in the first two atomic layers only, with fractions p_1 and p_2 of the first- and second-layer semiconductor atoms oxidized, respectively. The columnar model assumes a constant oxidized fraction p_O up to N layers. Two-layer models are closest to the actual oxide structure, and data for InP and GaAs are consistent with column structure models only for N less than or equal to 3.

The variation of the oxide fractional peak area with photon energy depends not only on the surface sensitivity of the photoemitted electrons, but also on how the oxidized atoms are distributed among the layers of the semiconductor lattice. In Fig. 12 two simplified structural models used for subsequent analysis are illustrated. In the first model the oxygen is assumed to be bound only to atoms in the first or second layer of the semiconductor crystal. The fraction of atoms in each layer which are oxidized is represented by the variables p_1 and p_2, for the first and second layers, respectively. A second oxide growth mode with more subsurface oxidation is modeled by columns of oxide which extend N layers deep and occupy a constant fraction p_O of each layer. The physical situation which this model tries to simulate is one where a defect or small fissure enhances the reactivity of a column of nearby atoms. Using these parameters and the electron inelastic-scattering lengths for the semiconductors, an expression for the oxide fractional peak area can be derived and, in turn, solved for one of the two parameters as a function of the other, i.e., $p_O(N)$ or $p_1(p_2)$. The experimentally determined values for the fractional peak area are used to generate a series of curves for different spectral kinetic-energy ranges, and the intersection of these curves is a self-consistent solution for the structural model and the data. For details of the derivation and graphical solution process the reader is referred to Ref. 35.

What we find for both GaAs and InP is that the two-layer model gives the best fit to the data, although the solution is not sensitive enough to distinguish between structures represented by ($p_1=1.0, p_2=0.2$), ($p_1=0.8$, $p_2=0.4$), and ($p_1=1.0, p_2=0.5$), for example. Attempts to fit the data with the column model yield values for the number of oxidized layers N between 1 and 3, thus confirming the validity of the two-layer model. One of the larger sources of ambiguity in these determinations is the lack of accurate inelastic-scattering-length data. Although the surface-shift values measured for this data and in work by others (see below) give limits for reasonable values, these are available for only a few kinetic energies mostly clustered around the escape-depth minimum. Universal curves such as those of Seah and Dench[48] or Lindau and Spicer[49] are also of limited use since the scatter from material to material is broad. The approach taken here is to allow for a range of inelastic-scattering-length values and report the resulting uncertainty in structural parameters.

The structural model calculations can, in turn, be inverted to provide a measure of the inelastic-scattering lengths, the results of which are given in Fig. 11(b). The values based on the data from this paper are in good agreement with those measured with other techniques, including the value of 4.2 Å at the scattering-length minimum derived from surface-shifted peaks in Sec. V A. Eastman *et al.*[31] and Landgren *et al.*[20] report a higher scattering length (6 Å) at the minimum, but as discussed previously this difference is due to a difference in electron-detection geometry. Other experimenters[11,50] have been able to correct for these effects, however, and still report slightly larger escape depths, although not beyond the experimental uncertainties in Fig. 11(b). One possible source of systematic error in the data presented here is an increase in the distance between the first and second atomic layers of the semiconductor caused by oxi-

dation. This hypothesis would explain why the scattering lengths measured for oxide layers are reproducibly low. [The values (not shown) of Pianetta *et al.*,[9] also taken from oxide layers, are in excellent agreement with the data in this paper when Pianetta's data are corrected for two errors[51] in the original analysis—one, normal emission was assumed when, in fact, a CMA had been used, and, two, that the layer thickness was taken as 4 Å instead of 2 Å.]

The differences between the shape of the InP and GaAs inelastic-scattering-length curves are a good illustration of how genuine differences in inelastic-scattering lengths can be found with this method. Although the error bars for the two curves do overlap, most of the error is systematically dependent on the structure assumed and, as a result, preserves the difference in the shape of the scattering-length–versus–kinetic-energy curve. This difference in shape is more clearly visible in Fig. 13, where the error bars are omitted and a logarithmic kinetic-energy scale is used. Within the structural models described above it is not possible to find a solution for InP based on the inelastic-scattering curve for GaAs or vice versa. The difference can be understood, however, by considering the scattering mechanisms involved. For electron energies in the range of 15 eV or more, the dominant energy-loss mechanism is the creation of electron-hole pairs from electron-electron scattering. The creation of such pairs depends on the density of initial and final states with the proper energy difference in much the same way that photoionization cross sections do. In the calculations of Yeh and Lindau[52] the photoionization cross sections for Ga and As are dominated by strong broad peaks associated with the 3*d* core levels with maxima at about 80 and 120 eV, respectively. Scattering in this energy range should therefore be efficient and less energy dependent, as is observed in Fig. 13.

For InP on the other hand, the In 4*d* core level dominates, since the In 3*d* level is too deep to be of influence, and P, having no 3*d* levels, can only contribute a weaker 2*p* cross section after its rapid onset at 135 eV. The 4*d* level has a qualitatively different energy dependence than 3*d* core levels, however, in that it goes through a Cooper minimum in cross section at about 120 eV caused by destructive interference between the 4*d* initial state and the outgoing-electron final state. The result is a cross section which peaks around 50 eV, then drops 2 orders of magnitude by 120 eV, never to recover the strong adsorption characteristic of 3*d* states. Electron scattering in InP should therefore be most efficient around 50 eV and then decrease rapidly in effectiveness relative to GaAs. These trends are precisely what is observed in the scattering lengths derived from oxide-structure modeling. The correlation between photoionization cross section and inelastic-scattering length is further supported by scattering-length values[50] for Ge. Germanium, lying in between Ga and As in the same row of the Periodic Table, has a core-level structure and photoionization-energy dependence similar to that of GaAs. The scattering lengths of Ge and GaAs, illustrated in Fig. 13, are much more alike than those of GaAs and InP, compounds whose constituent atoms have quite different photoionization-energy dependencies.

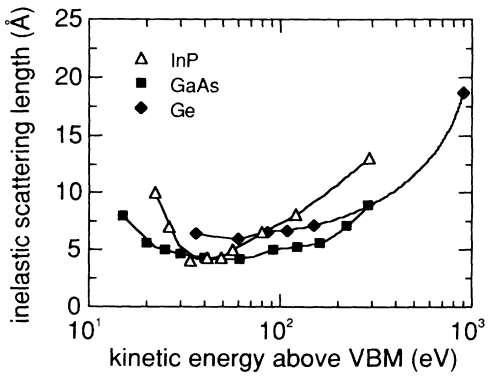

FIG. 13. Electron inelastic-scattering lengths vs the logarithm of the electron kinetic energy. Data (Ref. 50) on Ge are included to illustrate the relationship between electron inelastic-scattering length and photoionization cross sections.

VIII. DISCUSSION

A. Comparison with other experiments

The model of oxygen growth structure on InP and GaAs suggested by the experiments discussed here, then, is one in which oxygen chemisorbs primarily to the surface atoms, with equal bonding to the anions and cations at least up to a coverage of 1 ML. The layer-by-layer growth mode agrees with the work of Bartels and Mönch[53] in which the electron takeoff angle is varied for photoemission with two different x-ray photon energies. The use of different angles has one advantage over variation of photon energy in that the interpretation is less dependent on the absolute value of the inelastic-scattering length. Both experiments, however, were stimulated by the work of Landgren *et al.*,[20] who conclude that oxygen reacts to differing degrees with Ga and As and that the Ga oxide extends over 10 layers into the surface. There are two reasons why the results reported here and by Bartels and Mönch are more likely to be correct. First, the analysis used by Landgren to derive the 10-layer figure is incorrect in assuming that electrons collected are leaving the surface in the normal direction, since the actual electron-detector acceptance includes angles from normal emission to grazing emission. Second, Landgren's result is based on curve fitting for a small-shift peak in the Ga 3*d* spectra measured at only two kinetic energies. As demonstrated here, there are many uncertainties in identification and area determination of Ga peaks, while the As 3*d* data are less problematic to analyze, cover a large kinetic-energy range, and clearly lead to the opposite conclusion. Similar objections concerning the reliability of curve fitting for small-shift peaks have been raised by Miller and Chiang,[32] who report low-coverage oxygen chemisorption data for GaAs.

There are, of course, several possible sources of the disagreement, some of which have been eliminated from consideration. Because surface-dominated oxidation is supported by work on oxygen chemisorption at room

temperature in the dark,[9,53] the layer-by-layer growth mode is not merely representative of the optically enhanced oxygen chemisorption conditions used here. Landgren *et al.* explain their previously unobserved degree of subsurface oxidation and unusually low oxygen uptake by hypothesizing a strong dependence of oxygen uptake on microfissures or other defects created during cleaving. The differences from the work of others is then attributed to the variations in cleave quality from laboratory to laboratory, which implies that cleaving is unsuitable as a reproducible method of surface preparation. If such microfissures or defects did exist and influence oxygen chemisorption growth structure, however, they would have been detected by the As 3*d* experiments described in this paper. On the other hand, a less dramatic form of subsurface growth involving only the second and possibly third layers as well as the surface layer is consistent with the As 3*d* and O 1*s* results here and may provide an explanation for indications of subsurface oxidation. The differences in appearance of the raw data may be exaggerated by the previously mentioned difference in electron-detection geometry. Angular effects such as electron refraction and diffraction could be particularly important at low kinetic energies, where one of Landgren's two key spectra are taken. (See Miller *et al.*[54] for an example of angular effects in photoemission from germanium surfaces.)

A second question under consideration is whether or not oxygen chemisorbs in more than one phase as the coverage increases. The identification of more than one shifted peak and the recognition of broadening induced by oxidation were first discussed and quantified by Landgren *et al.*, and our data concur with the existence of multiple peaks and broadening. These features are relevant to any model for the oxide structure, since they point to a degree of disorder and variation in bonding sites which raises serious doubts that the oxygen is confined only to surface bonds or dangling bonds. The peak identifications developed in this paper, however, disagree with an interpretation in which all shifted peaks are attributed to direct oxygen bonding. The difference in peak identifications is the chief factor leading to our model of oxidation in which Ga and As are involved to an equal extent and therefore likely to be forming a single oxide phase rather than forming separate phases with different growth rates. This change is supported by the superior correlation between O 1*s* emission and large-shift peak areas, and the larger contributions of the shifted peaks to the overall spectra in our data, thereby increasing the reliability of curve fitting. As pointed out earlier, a single-phase growth mode is also more likely at room temperature due to kinetic limitations.

B. Suggestions for future work

Since the use of higher-resolution spectroscopy has failed to identify unambiguously the structure of oxygen chemisorbed on GaAs(110), future work along the same lines will probably not be very productive. The phenomena which produce binding-energy shifts in photoemission are not understood well enough to make structural determinations by merely counting up peaks delineated by a curve-fitting routine. Even further improvements in photon- and electron-energy resolution are unlikely to clarify the situation since surface disorder is already the largest source of peak broadening. A more promising approach is to use an angle-resolved technique and thereby gain greater structural sensitivity. As an incentive to those who might pursue such an approach, Fig. 14 demonstrates how the oxygen features in the valence band are sensitive to the polarization of light used to excite photoemission. Low-energy spectroscopies such as infrared-absorption or high-resolution electron-energy-loss spectroscopy may also be helpful because of their superior ability to resolve small bond-energy differences.

IX. SUMMARY

Synchrotron- and standard x-ray-photoemission data have been used to model the growth structure for oxygen chemisorption on GaAs(110) and, to a lesser extent, InP(110). High-resolution core-level spectra are examined critically to determine the surface sensitivity for the experimental configuration and to identify peaks in the spectra which correspond to semiconductor atoms directly bonded to oxygen. Only peaks with large binding-energy shifts are attributed to direct oxygen bonding, while peaks with smaller shifts are presumed to arise from the same kinds of structural relaxation and nearest-neighbor charge-transfer effects which give rise to surface shifts. The relative contributions of the oxidized and unoxidized atoms to the As 3*d* and P 2*p* spectra at different photoemission probing depths support a model in which the oxide grows more or less homogeneously, layer by layer, and are inconsistent with an oxide four or more atomic layers deep. O 1*s* data corroborate the structure model and peak identifications. Although the surface oxide model contradicts some similar early work

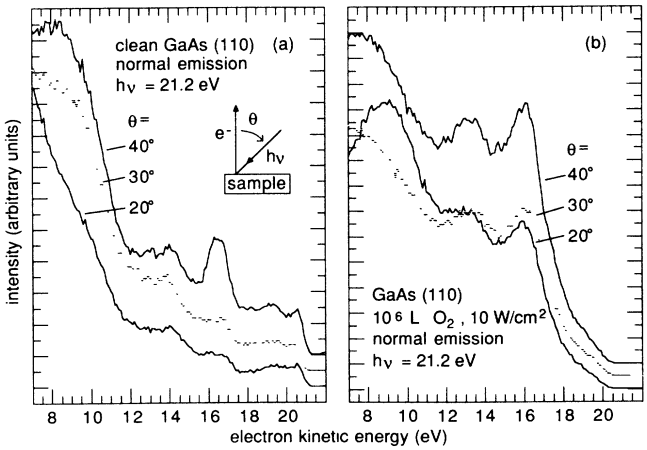

FIG. 14. Polarization dependence of valence-band structure for clean and oxidized GaAs(110) using angle-resolved photoemission. The oxygen feature at 16 eV is seen to increase relative to the semiconductor features as the angle of incidence θ increases. This change could indicate a dipole perpendicular to the surface, as increasing the angle of incidence increases the perpendicular component of the vector potential of the incoming light wave.

on this system, the approach taken in this paper avoids a number of problems in those experiments and thereby lends further support to a surface oxygen chemisorption model for GaAs and InP.

ACKNOWLEDGMENTS

The assistance of C. E. McCants, M. D. Williams, T. T. Chiang, and R. S. List in acquiring some of the data discussed in this paper is gratefully acknowledged. This research is supported by the Defense Advanced Research Projects Agency and the U. S. Office of Naval Research under Contract No. N00014-83-K-0073. The Stanford Synchrotron Radiation Laboratory is supported by the U. S. Department of Energy, Office of Basic Energy Sciences, and the National Science Foundation, Division of Materials Research.

APPENDIX: O 1*s* ANALYSIS

In this work O 1*s* data are interpreted quantitatively by measuring the peak areas under the relevant photoemission peaks and then correcting for differences in peak areas which arise from factors independent of the concentration of chemical species on the surface, namely the x-ray–source intensity, the electron-energy-analyzer transmission and image diameter, the photoionization cross section, and the sampling depth (related to the inelastic-scattering length and concentration profile). Table III gives the values for these corrections, and this appendix outlines their derivation. A more complete explanation can be found in Ref. 38.

The x-ray photon intensity is a difficult number to obtain directly and therefore peak-area *ratios* of oxygen emission to gallium and arsenic emission are used rather than absolute values. Ideally, the semiconductor XPS spectra should be taken at each exposure, but time did not always permit such complete investigation. The background level on the high-kinetic-energy side of the oxygen peak has been used instead to correct for intensity changes due to sample positioning or fluctuation in the photon flux produced by the x-ray source. The ratio of background counts to the semiconductor peak areas is determined for at least one exposure in each series (usually the clean spectrum) to provide an anchor point for subsequent corrections. This procedure gives a_O:a_{Ga} peak-area ratios within 10% of those measured from actual peaks in an exposure series for which complete XPS data is available. This correction sets the amount of random error in the experimental data to 10% since it far outweighs the variations in peak area for different determinations of the peak areas.

The response of the cylindrical mirror analyzer (CMA) used to measure the electron-energy distributions has been thoroughly discussed by other authors.[55,56] The peak areas are multiplied by the mean kinetic energy of the peak to correct for changes in the image area. No further corrections are needed for XPS 3*d* spectra since they are taken with the analyzer pass energy (50 eV) used for the O 1*s* spectra; the As 2*p* and Ga 2*p* spectra from Al $K\alpha$ x rays, however, are taken with a smaller pass energy (25 eV). Rather than apply several theoretical corrections, the 2*p* peak areas are converted to equivalent 3*d* spectral areas taken at higher pass energy by factors of 0.14 ± 0.02 and 0.17 ± 0.02 for As and Ga, respectively, as empirically determined from 2*p* and 3*d* spectra taken with the appropriate pass energies on the same surfaces.

The photoionization cross-section correction also consists of two parts—the total probability of photoionization for a particular core level and an asymmetry adjustment to correct for the asymmetrical angular distribution of the emitted electrons. The total cross sections are taken from Yeh and Lindau[52] and are virtually identical to earlier work[57] by Scofield. In addition, Yeh and Lindau calculate the asymmetry parameter β, which allows determination of the effective cross section σ_{eff} for a particular electron-detection geometry. This calculation has been done[56] for the detector geometry used in this work with the result

$$\sigma_{\text{eff}}=\frac{\sigma}{4\pi}(1+\delta\beta),\quad \delta=0.29\ . \tag{A1}$$

The factor $1+\delta\beta$ is given as the asymmetry correction in Table III; the peak areas are corrected by dividing each area by the product of the total cross section and the asymmetry correction.

The adjustments for inelastic-scattering length and nonuniform oxygen distribution are the most difficult corrections to estimate. Even if atoms are distributed

TABLE III. Corrections for O 1*s* peak areas. $G(L)$ factors for oxygen are calculated using an oxide thickness of 2 Å.

Core level	Photon energy (eV)	Kinetic energy (eV)	Total cross section (Mb)	Asymmetry correction	Inelastic-scattering length (Å)	$G(L)$	Total correction
O 1*s*	1253.6	717	0.063	1.58	18	9.92	71.5
O 1*s*	1486.6	951	0.040	1.58	21	10.6	159.5
Ga 3*d*	1253.6	1230	0.026	1.31	25	$\equiv 1.0$	36.1
Ga 3*d*	1486.6	1462	0.014	1.29	27	$\equiv 1.0$	81.0
As 3*d*	1253.6	1208	0.044	1.32	24	1.04	21.6
As 3*d*	1486.6	1441	0.025	1.31	26	1.04	45.8

uniformly in depth to several scattering lengths into the crystal, as are the Ga and As atoms, the effective volume sampled will still be different for different peaks. This difference arises from the fact that, for emission at kinetic energies with a longer scattering length, photoexcited electrons from more layers will reach the detector and produce a peak with greater intensity. The volume sampled per surface area is directly proportional to the inelastic-scattering length L, as shown by integrating the contributions to the total peak intensity (= area) I from thin layers with thickness dz located at a distance z from the surface:

$$I = A\int_0^\infty (\rho d)e^{-z/L\cos\theta}dz = A(\rho d)L\cos\theta\ , \qquad \text{(A2)}$$

where ρd is the atomic density per unit area given by the volume density ρ times the interlayer spacing d, θ is the angle between the electron path and the sample normal, and A corrects for the other factors already discussed. The appropriate scattering-length correction, then, is to divide the Ga and As peak areas by the corresponding inelastic-scattering lengths; for calculational convenience, in the actual correction factor $G(L)$ is normalized to the Ga correction. The factor of $\cos\theta$ cancels in taking peak-area ratios since the electron-detection geometry is the same for all spectra.

For a thin oxide layer this description is complicated by the fact that the oxygen only reaches a distance D into the crystal which is less than a single inelastic-scattering length for the O 1*s* core-level emission. To account for this structure, the oxygen is assumed to be distributed uniformly in depth throughout the oxide layer. The oxygen peak area expected from the oxide layer alone is given by the same integral in Eq. (3) with the upper limit replaced by the oxide thickness D, giving the result that the peak intensity should be proportional to $p_O L_O\cos\theta\{1-\exp[-D/(L_O\cos\theta)]\}$, where p_O is the area density of oxygen in each layer. Normalizing this correction to the Ga correction yields the inelastic-scattering-length correction for oxygen $G_O(L_O) = (L_{Ga}/L_O)(1-e^{-D/L_O\cos\theta})^{-1}$. The values in Table III assume an oxide thickness of 2Å, or one lattice plane spacing in the [110] direction. Although $G_O(L_O)$ is reduced by a factor of 0.535 for a 4-Å oxide layer and continues to fall as oxide thickness increases, the oxide fractional peak area for the As 3*d* peak sets a lower limit on the oxygen coverage of 0.5 ML in each layer (at the highest exposures), which restricts the range of possible thicknesses to less than or perhaps equal to 4 Å. The O 1*s* coverage values in Fig. 8 are derived by averaging the values for a 2-Å oxide layer and a 4-Å layer, and the dashed lines indicate the ±27% variations required to span the range between these two coverages.

The total correction given in Table III is number by which each peak area should be multiplied to get a number directly proportional to the area density of each species. The oxide coverage in monolayers is then the ratio of the corrected oxygen peak intensity to the sum of corrected Ga and As peak intensities.

The accuracy of this technique can be gauged by the measure of the relative amounts of gallium and arsenic from a clean, cleaved sample. Area-density determinations from 3*d* core levels and corrected 2*p* data consistently indicate ≈15% more Ga than As. Since the appearance of a Ga excess persists for samples from several different ingots, the most likely explanation would be a systematic error in the cross-section calculations. Although one could argue that the process of cleaving might result in some loss of arsenic from the surface, such a loss would not be readily apparent in the 3*d* XPS measurements since these spectra reflect an average in composition over more than 50 Å into the sample. The cross-section calculations therefore have an estimated uncertainty of ±15%. While relatively large, this uncertainty is still significantly less than the uncertainty arising from the imprecise knowledge of the oxide layer thickness.

*Present address: Varian Associates Research Center (Mail Stop K221), 611 Hansen Way, P.O. Box 10800, Palo Alto, CA 94303-0883.

[1]R. Dorn, H. Lüth, and G. J. Russell, Phys. Rev. B **10**, 5049 (1974).

[2]A. Kahn, D. Kanani, P. Mark, P. W. Chye, C. Y. Su, I. Lindau, and W. E. Spicer, Surf. Sci. **87**, 325 (1979).

[3]Eugene J. Mele and J. D. Joannopoulos, Phys. Rev. B **18**, 6999 (1978).

[4]C. Y. Su, I. Lindau, P. W. Chye, P. R. Skeath, and W. E. Spicer, Phys. Rev. B **25**, 4045 (1982). The calculation of the nonbonding-bonding energy shift expected for an As=O bond in the paper of Su *et al.* is in error, however; the correct value should be 6.62 eV instead of 3.36 eV.

[5]G. Hughes, R. Ludeke, J. F. Morar, and J. L. Jordan, J. Vac. Sci. Technol. B **3**, 1079 (1985).

[6]G. Hughes and R. Ludeke, J. Vac. Sci. Technol. B **4**, 1109 (1986).

[7]P. Pianetta, I. Lindau, C. M. Garner, and W. E. Spicer, Phys. Rev. Lett. **35**, 1356 (1975).

[8]R. Ludeke, Solid State Commun. **21**, 815 (1977).

[9]P. Pianetta, I. Lindau, C. M. Garner, and W. E. Spicer, Phys. Rev. B **18**, 2792 (1978).

[10]W. Ranke and K. Jacobi, Surf. Sci. **63**, 33 (1977).

[11]W. Ranke and K. Jacobi, Prog. Surf. Sci. **10**, 1 (1981).

[12]P. W. Chye, P. Pianetta, I. Lindau, and W. E. Spicer, J. Vac. Sci. Technol. **14**, 917 (1977).

[13]F. Bartels, L. Surkamp, H. J. Clemens, and W. Mönch, J. Vac. Sci. Technol. B **1**, 756 (1982).

[14]C. R. Brundle and D. Seybold, J. Vac. Sci. Technol. **16**, 1186 (1979).

[15]D. J. Frankel, Y. Yukun, R. Avci, and G. J. Lapeyre, J. Vac. Sci. Technol. A **1**, 679 (1983).

[16]D. J. Frankel, J. R. Anderson, and G. J. Lapeyre, J. Vac. Sci. Technol. B **1**, 763 (1983).

[17]J. Stöhr, R. S. Bauer, J. C. McMenamin, L. I. Johansson, and S. Brennan, J. Vac. Sci. Technol. **16**, 1195 (1979).

[18]P. J. Grunthaner, R. P. Vasquez, and F. J. Grunthaner, J.

Vac. Sci. Technol. **17**, 1045 (1980).
[19]F. Bartels and W. Mönch, Surf. Sci. **143**, 315 (1984).
[20]G. Landgren, R. Ludeke, Y. Jugnet, J. F. Morar, and F. J. Himpsel, J. Vac. Sci. Technol. B **2**, 351 (1984).
[21]P. W. Chye, C. Y. Su, I. Lindau, C. M. Garner, P. Pianetta, and W. E. Spicer, Surf. Sci. **88**, 439 (1979).
[22]K. A. Bertness, T. Kendelewicz, R. S. List, M. D. Williams, I. Lindau, and W. E. Spicer, J. Vac. Sci. Technol. A **4**, 1424 (1986).
[23]G. Hollinger, G. Hughes, F. J. Himpsel, J. L. Jordan, and J. F. Morar, and F. Houzay, Surf. Sci. **168**, 617 (1986).
[24]G. Hollinger, E. Bergignat, J. Joseph, and Y. Robach, J. Vac. Sci. Technol. A **3**, 2082 (1985).
[25]J. F. Wager, K. M. Geib, C. W. Wilmsen, and L. L. Kazmerski, J. Vac. Sci. Technol. B **1**, 778 (1983).
[26]C. W. Wilmsen, J. Vac. Sci. Technol. **19**, 279 (1981).
[27]G. P. Schwartz, W. A. Sunder, and J. E. Griffiths, J. Electrochem. Soc. **129**, 1361 (1982).
[28]Winfried Mönch, Surf. Sci. **168**, 577 (1986).
[29]R. M. Feenstra and A. P. Fein, Phys. Rev. B **32**, 1394 (1985).
[30]Joseph A. Stroscio, R. M. Feenstra, and A. P. Fein, Phys. Rev. Lett. **58**, 1668 (1987).
[31]D. E. Eastman, T.-C. Chiang, P. Heimann, and F. J. Himpsel, Phys. Rev. Lett. **45**, 656 (1980).
[32]T. Miller and T.-C. Chiang, Phys. Rev. B **29**, 7034 (1984).
[33]A. Ismail, J. M. Palau, and L. Lassabatere, J. Appl. Phys. **60**, 1730 (1986).
[34]P. Pianetta, I. Lindau, P. E. Gregory, C. M. Garner, and W. E. Spicer, Surf. Sci. **72**, 298 (1978).
[35]K. A. Bertness, D. J. Friedman, P. H. Mahowald, J. J. Yeh, A. K. Wahi, I. Lindau, and W. E. Spicer, J. Vac. Sci. Technol. B **4**, 1102 (1986).
[36]W. G. Petro, I. Hino, S. Eglash, I. Lindau, C. Y. Su, and W. E. Spicer, J. Vac. Sci. Technol. **21**, 405 (1982).
[37]K. A. Bertness, T. T. Chiang, C. E. McCants, P. H. Mahowald, A. K. Wahi, T. Kendelewicz, I. Lindau, and W. E. Spicer, Surf. Sci. **185**, 544 (1987).
[38]Kristine A. Bertness, Ph.D. thesis, Stanford University, 1987.
[39]G. Leonhardt, A. Berndtsson, J. Hedman, M. Klasson, R. Nilsson, and C. Nordling, Phys. Status Solidi B **60**, 241 (1973).
[40]M. K. Bahl, R. O. Woodall, R. L. Watson, and K. J. Irgolic, J. Chem. Phys. **64**, 1210 (1976).
[41]J. W. Davenport, R. E. Watson, M. L. Perlman, and T. K. Sham, Solid State Commun. **40**, 999 (1981).
[42]John J. Barton, William A. Goddard III, and T. C. McGill, J. Vac. Sci. Tecnol. **16**, 1178 (1979).
[43]The net amount of charge transferred to chemisorbed oxygen from GaAs has been reported as $-0.28e$ per oxygen atom, where e is the magnitude of the charge of one electron. See W. Mönch and R. Enninghorst, J. Vac. Sci. Technol. **17**, 942 (1980).
[44]G. Lucovsky, J. Vac. Sci. Technol. **19**, 456 (1981).
[45]C. D. Thurmond, G. P. Schwartz, G. W. Kammlott, and B. Schwartz, J. Electrochem. Soc. **127**, 1366 (1980).
[46]This restriction can be understood by imagining an oxide which includes half the semiconductor atoms in each layer down to a depth of several inelastic-scattering lengths. The oxide fractional peak area of the As $3d$ peak would then be equal to the fraction of each layer which is oxidized, or 0.5. If the oxide does not extend so deeply, the oxide fractional peak area will only become smaller, as more of the atoms detected will be unoxidized.
[47]Piero Pianetta, I. Lindau, and W. E. Spicer, *Quantitative Surface Analysis of Materials*, ASTM Special Technical Publication No. 643, edited by N. S. McIntyre (American Society for Testing and Materials, Philadelphia, PA, 1978).
[48]M. P. Seah and W. A. Dench, Surf. Interface Analy. **1**, 2 (1979).
[49]I. Lindau and W. E. Spicer, J. Electron Spectrosc. Relat. Phenom. **3**, 409 (1974).
[50]H. Gant and W. Mönch, Surf. Sci. **105**, 217 (1981).
[51]Perry Skeath, Ph.D. thesis, Stanford University, 1982.
[52]J. J. Yeh and I. Lindau, At. Data Nucl. Data Tables **32**, 1 (1985).
[53]F. Bartels and W. Mönch, Solid State Commun. **57**, 571 (1986).
[54]T. Miller, A. P. Shapiro, and T.-C. Chiang, Phys. Rev. B **31**, 7915 (1985).
[55]Perkin-Elmer Corporation, Instruction Manual PHI model 15-255G Precision Electron Energy Analyzer (Perkin-Elmer Corp., Eden Prairie, MN, 1975).
[56]Michael H. Hecht, Ph.D. thesis, Stanford University, 1982, p. 86.
[57]J. H. Scofield, J. Electron Spectrosc. Related Phenom. **8**, 129 (1976).

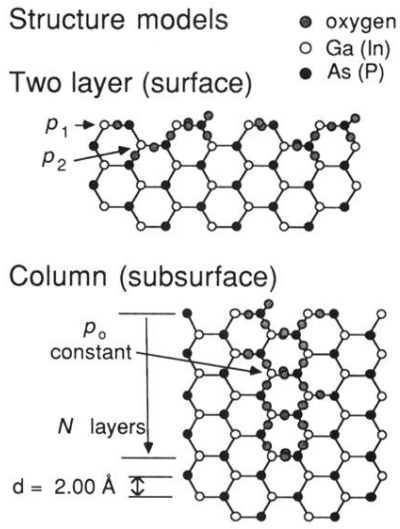

FIG. 12. Oxide-growth models, two layer and columnar. The two-layer models assume that oxygen is present in the first two atomic layers only, with fractions p_1 and p_2 of the first- and second-layer semiconductor atoms oxidized, respectively. The columnar model assumes a constant oxidized fraction p_O up to N layers. Two-layer models are closest to the actual oxide structure, and data for InP and GaAs are consistent with column structure models only for N less than or equal to 3.